buildings

MDPI

Article

Study on Damping Performance of Hyperboloid Damper with SMA-Negative Stiffness

Huahui Chang [1], Leifei Liu [1], Li Jing [1], Jingyan Lu [1] and Sasa Cao [2,*]

[1] School of Civil Engineering, Shangqiu Institute of Technology, Shangqiu 476000, China; 2111716081@e.gzhu.edu.cn (H.C.); liuleifei2012@126.com (L.L.); jingli9410@163.com (L.J.); lujy_123456@126.com (J.L.)
[2] School of Civil Engineering, Guangzhou University, Guangzhou 510006, China
* Correspondence: cao@gzhu.edu.cn

Abstract: To improve the limiting capacity of isolation bearings and reduce residual deformation, a new material shape memory alloy (SMA) was introduced into the damping device. SMA shape memory materials have shape memory effect, superelastic effect, and damping properties of metal alloys. Although the SMA isolation bearing can improve the self-resetting ability of the bridge, it will increase the internal force response of the substructure compared with the ordinary isolation bearing. To solve this problem, a new type of SMA negative stiffness hyperboloid shock absorber is proposed. The device is provided with restoring force by SMA cables, negative rigidity by two friction pendulum supports with opposite curved surfaces, and energy dissipation capacity by friction between the slider and the upper and lower steel plates. Theoretical derivation and finite element analysis results show that the damping device can not only provide the self-resetting ability of the bridge but also partially reduce the internal force response of the SMA damping bridge structural system on the premise of reducing the displacement response of the bridge.

Keywords: bridge; isolation bearing; negative stiffness; double inverted surfaces; superelastic shape memory alloy

check for updates

Citation: Chang, H.; Liu, L.; Jing, L.; Lu, J.; Cao, S. Study on Damping Performance of Hyperboloid Damper with SMA-Negative Stiffness. *Buildings* **2022**, *12*, 1111. https://doi.org/10.3390/buildings12081111

Academic Editor: Davor Stanko

Received: 4 July 2022
Accepted: 22 July 2022
Published: 28 July 2022

Publisher's Note: MDPI stays neutral with regard to jurisdictional claims in published maps and institutional affiliations.

Copyright: © 2022 by the authors. Licensee MDPI, Basel, Switzerland. This article is an open access article distributed under the terms and conditions of the Creative Commons Attribution (CC BY) license (https://creativecommons.org/licenses/by/4.0/).

1. Introduction

For the bridge structure system designed for seismic isolation, its fundamental period is far away from the predominant period of ground motion, and the internal force response of the structure is significantly reduced corresponding to the ductile bridge structure system. However, the earthquake tests in recent years have shown [1–4] that the limited capacity of seismic isolation bridges is insufficient, and there are still a large number of earthquake damages such as collisions, displacement of bearings, or falling beams [5–7]. To improve the restraint capacity and self-reset ability of seismic isolation bridges, shape memory alloy (SMA) materials are introduced into seismic isolation bridges [8,9]. The SMA member and the vibration isolation bearing form a new type of vibration isolation device, which can effectively reduce the maximum displacement and residual displacement of the bridge structure and improve its self-reset performance [10–16]. However, the introduced SMA limit system in turn increases the stiffness of the isolation device, and to a certain extent increases the internal force response of the bridge substructure. It is a new problem to be solved, how to increase the internal force of the bridge substructure while improving the self-recovery ability.

To reduce the internal force of SMA, Refs. [17–20] and Wang and Cao [21] proposed the multi-level fortified SMA lead bearing, which can reduce the structural internal force under moderate and strong earthquakes to a certain extent; the test shows that SMA has strong resilience. Han et al. [22] proposed a variable curvature SMA friction. The pendulum support subtly reduces the internal force response of the structure by reducing the curvature during large displacement. The core idea of the above two methods is to

reduce the stiffness of the bearing at large displacements. Active and semi-active seismic isolation devices can simultaneously reduce the internal force and displacement response of the structure [23–25], but these devices rely more or less on external power control, and the power supply facilities are easily damaged during earthquakes. Studies have shown [26,27] that in some active and semi-active structures, the force-displacement relationship of the control device exhibits negative stiffness characteristics.

Based on this phenomenon, Iemura et al. [28] proposed a new type of negative stiffness device, which can greatly reduce the displacement and acceleration response of the structure after the device is connected in parallel with ordinary rubber bearings to form a new isolation system. Attary et al. [29] simulated and analyzed structure of highway bridges with negative stiffness devices, and the results show that the device can not only maintain the structural stability but also greatly reduce structural stiffness. Subsequently, Attary et al. [30] conducted a shaking table test on a new type of negative-stiffness device, which confirmed that the negative-stiffness system was significantly better than the positive-stiffness system in reducing the structural response. In China, Deng et al. [31] study shows that the SMA-based bearing has an excellent re-centering capacity and displacement-limiting capacity. Shao and Cao [32] and Chang et al. [33] show that the negative stiffness device can effectively increase the damping ratio and energy dissipation capacity of the structural system, thereby significantly reducing the internal force of the structure. Sun et al. [34] proposed a negative stiffness device composed of springs, rollers, and sliding rails, and verified its positive effect on reducing the seismic response of structures through experiments. In addition, Yang et al. [35] proposed a negative stiffness device with damping based on pre-compressed springs, spherical hinges, and obliquely rotating dampers. The device can not only reduce the acceleration response of the superstructure under the action of long and short-period earthquakes but also control the displacement response of the seismic isolation layer and improve the seismic isolation efficiency. Liu et al. [36] combined the negative stiffness device with SMA wire and proposed a recoverable negative stiffness system. They pointed out that the negative stiffness device can effectively increase the damping ratio and energy dissipation capacity of the structural system, thereby significantly reducing the internal force of the structure.

Based on the above research, this paper proposes a new type of SMA-negative stiffness hyperboloid shock absorber. First, the restoring force model of the SMA-negative stiffness hyperboloid shock absorber is theoretically analyzed; second, based on the finite element model, the key parameters affecting the SMA-negative stiffness hyperboloid shock absorber are analyzed; finally, taking a continuous girder bridge as an engineering example, the superiority of the hyperboloid isolator with SMA negative stiffness is verified.

2. SMA-Negative Stiffness Hyperboloid Shock Absorber

2.1. Design Principle

Although the damping system combined with the SMA cable and the traditional damping bearing can effectively improve the self-resetting ability of the structure, on the other hand, it also increases the internal force response of the structure. To provide the self-recovery ability and partially reduce the internal force response of the structure, a new type of SMA-negative stiffness hyperboloid isolation device is proposed based on the negative stiffness design concept. Its design concept is shown in Figure 1; k1 is the positive stiffness provided by the SMA cable system and k2 is the negative stiffness provided by the inverse hyperboloid bearing. On the one hand, when the negative stiffness device is added to the SMA damping system, the displacement response of the structure is significantly reduced; on the other hand, the negative stiffness effect will reduce the overall stiffness of the damping device, thereby partially reducing the internal force response of the structure.

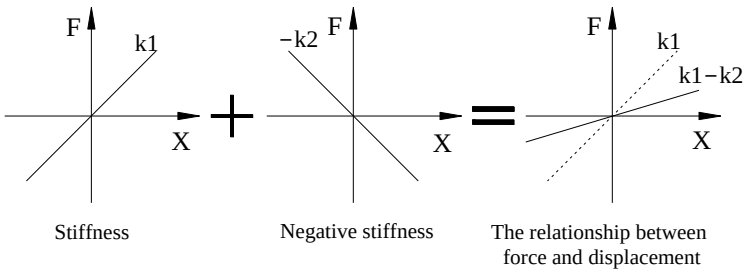

Figure 1. Design principle of negative stiffness hyperboloid damper.

2.2. Structure

The SMA-negative stiffness hyperboloid shock absorber is composed of SMA cables, upper and lower convex steel plates, and double concave sliders, as shown in Figure 2, and its cross-section is shown in Figure 3a. The SMA cable passes through the grooves of the upper and lower steel plates and is connected on one side of the support to form a ring arrangement. The SMA cable is placed in the grooves of the upper and lower steel plates and is not fixed in contact with the steel plate, allowing free sliding between the cable and the steel plate. The longitudinal and transverse groove depths are different to ensure that the SMA cables do not touch (see Figure 3b).

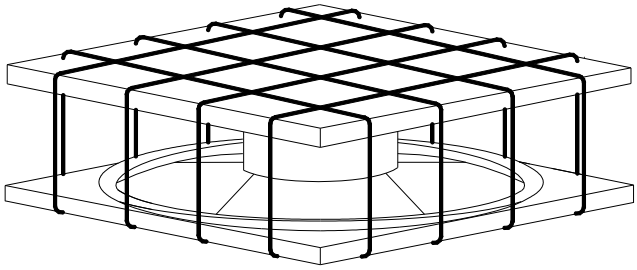

Figure 2. SMA negative stiffness hyperboloid shock absorber.

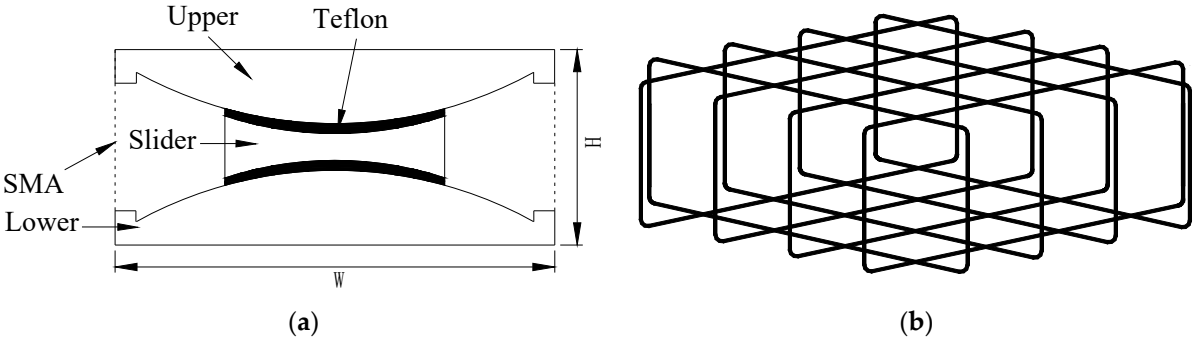

Figure 3. (**a**) Profile, (**b**) SMA cable layout.

2.3. Mechanism

Figure 4 is the force analysis diagram of the negative stiffness hyperboloid shock absorber. W is the pressure transmitted from the upper structure to the upper steel plate; R is the curved surface radius of the upper and lower plates; x is the horizontal displacement of the shock absorber (rightward is positive); θ is the rotation angle of the contact center of the steel plate on the support along the curved surface when the relative displacement from the support is 0 to x; N is the reaction force of the slider on the sliding surface; N_h is the horizontal force generated by the negative stiffness device; F is the friction force on the friction surface; μ is the friction factor of the two sliding surfaces; $\ddot{Z}$ is the ground motion acceleration; $\ddot{X}$ is the relative acceleration of the main beam; and g is the acceleration of gravity.

Iemura and Pradono [37,38] pointed out that the motion equation of the negative stiffness device under the action of the earthquake is:

$$x = Rsin\theta \tag{1}$$

$$\frac{W}{g}\ddot{x} + F(x,\dot{x}) = -\frac{W}{g}\ddot{z} \tag{2}$$

$$F(x,\dot{x}) = -N_h + \mu \cdot W \cdot sgn(\dot{x})cos\theta \tag{3}$$

In the formula, $sin\theta = \frac{X}{R}$, $sgn(x)$ is the sign function of the motion speed. When $x > 0$, $sgn(x) = 1$; when $x < 0$, $sgn(x) = -1$. Because x is very small relative to R, then θ is very small, so $cos\theta \approx 1$, so Equation (3) can finally be simplified as:

$$F(x,\dot{x}) = -N_h + \mu \cdot W \cdot sgn(\dot{x}) \tag{4}$$

In the formula, the expression of N_h is

$$N_h = Wsin\theta cos\theta \tag{5}$$

To simplify the calculation, some components of the SMA-negative stiffness hyperboloid shock absorber are simplified in Figure 5. y is the vertical displacement of the upper steel plate; L_0 and L are the initial and tensile lengths of the vertical section of the SMA cable, respectively; and α is the angle between the cable and the bottom plate after deformation.

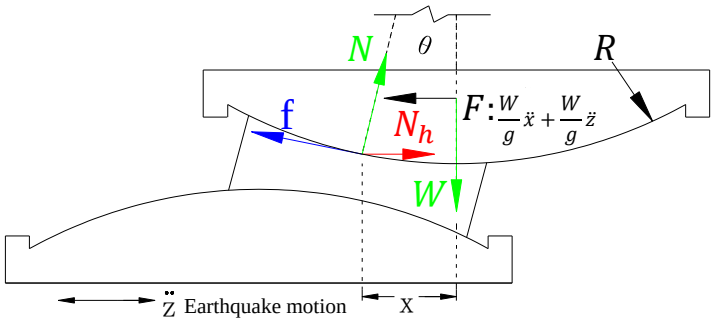

Figure 4. Stress analysis diagram of negative stiffness bearing under earthquake action.

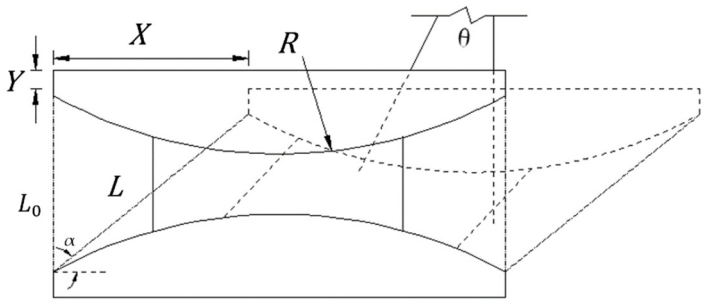

Figure 5. The simple calculation of SMA negative stiffness hyperboloid bearing.

x and y represent the horizontal and vertical displacement of the device movement, respectively; then:

$$Y = R(1 - cos\theta) \tag{6}$$

$sin\theta = \frac{x}{R}$, and θ is very small, then $\theta \approx sin\theta \approx \frac{x}{R}$, we can obtain:

$$Y = R(1 - cos\frac{x}{R}) \tag{7}$$

The stretched SMA is:

$$L = \sqrt{x^2 + (L_0 - Y)^2} \tag{8}$$

SMA cable elongation ΔL is:

$$\Delta L = L - L_0 = \sqrt{x^2 + (L_0 - Y)^2} - L_0 \tag{9}$$

The strain value of the SMA cable is:

$$\varepsilon = \frac{\Delta L}{L} = \sqrt{x^2 + (L_0 - Y)^2}/L_0 - 1 \tag{10}$$

Then the restoring force of the SMA cable is:

$$F_{\mathrm{SMA}} = nA\sigma(\varepsilon) \tag{11}$$

In the formula, n is the number of vertical segments of SMA cables, A is the cross-sectional area of each SMA cable; $\sigma(\varepsilon)$ is the stress of the SMA cable. First obtain ε according to formula (10), and then obtain σ from the constitutive relation of SMA.

$$\text{Level}: F^H_{\mathrm{SMA}} = F_{\mathrm{SMA}} cos\alpha \tag{12}$$

$$\text{Vertical}: F^V_{\mathrm{SMA}} = F_{\mathrm{SMA}} sin\alpha \tag{13}$$

In the formula, α is the angle between the cable and the bottom plate after deformation; there are:

$$cos\alpha = \frac{x}{\sqrt{x^2 + [L_0 - R(1 - cos\frac{x}{R})]^2}} \tag{14}$$

$$sin\alpha = \frac{L_0 - R(1 - cos\frac{x}{R})}{\sqrt{x^2 + [L_0 - R(1 - cos\frac{x}{R})]^2}} \tag{15}$$

The total restoring force in the horizontal direction of the negative stiffness hyperboloid shock absorber is the sum of the horizontal component force of the SMA system and the horizontal component force of the negative stiffness system. According to Equations (4), (5), and (12), we can get:

$$F = F_{\mathrm{SMA}} cos\alpha - W cos\theta cos\alpha + \mu W sgn(\dot{x}) \approx F_{\mathrm{SMA}} cos\alpha - W\frac{x}{2R} + \mu W sgn(\dot{x}) \tag{16}$$

It can be seen from Equation (16) that the restoring force of the SMA-negative stiffness hyperboloid shock absorber is composed of three parts: the restoring force provided by the SMA cable, the negative stiffness provided by the inverse hyperboloid friction pendulum bearing, and the sliding surface friction force, where the negative stiffness is $\frac{W}{2R}$.

3. Hysteretic Performance of SMA-Negative Stiffness Hyperboloid Shock Absorber

SMA-negative stiffness hyperboloid shock absorbers provide self-reset capability via superelastic SMA cables. The device to be designed is a $7 \times 7 \times 0.885$ mm superelastic NiTiSMA cable produced by the FortWayne Company in the United States (see Figure 6). Ozbulut et al. [39] tested the stress-strain relationship of the same type of cable. For the convenience of calculation, according to their experimental results, referring to the constitutive model of Auricchio and Taylor [40], the stress-strain model of SMA material is simplified to a flag shape as shown in Figure 7.



Figure 6. Superelastic NiTi SMA cable.

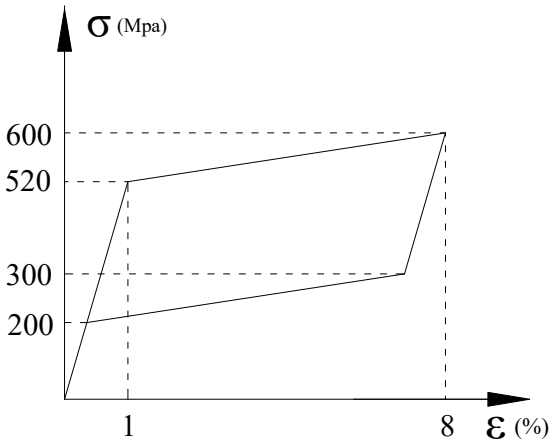

Figure 7. SMA cable stress and strain model.

3.1. Restoring Forces and Displacements of SMA Cables and Negative Stiffness Systems

To better study the horizontal restoring force of the SMA negative stiffness hyperboloid shock absorber, first analyze the horizontal restoring force of the SMA cable and the restoring force of the negative stiffness system. According to Figure 7, when the SMA strain is 8%, the horizontal displacement is 81 mm, and W = 3000 kN, μ = 0.02, R = 3 m, r = 8 mm, the restoring force-displacement of the SMA cable and the negative stiffness system is obtained as shown in Figure 8 below. The horizontal restoring force of the SMA negative stiffness hyperboloid shock absorber is formed by the superposition of the two.

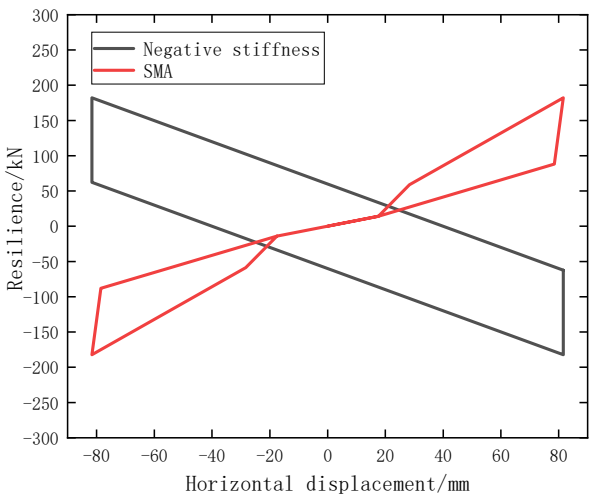

Figure 8. Restoring force-displacement comparison of SMA cable and negative stiffness system.

3.2. Numerical Simulation

Based on ANSYS software, the finite element model of the SMA-negative stiffness hyperboloid shock absorber is established, as shown in Figure 9. Among them, the upper and lower steel plates and sliders are simulated by 185 elements. To accurately simulate the deformation behavior of SMA cables arranged in a hoop, it is difficult to simultaneously consider the material nonlinearity, geometric nonlinearity, large de-formation effect of SMA cables, and contact nonlinearity between the cables and the upper and lower steel plates. To reduce the computational difficulty and the amount of computation, a simplified method is used to simulate the SMA cable. The principle of simplification is: on the one hand, the effective cross-sectional area of the SMA cable before and after the simplification is required to be the same; on the other hand, according to the ratio of the length of the straight cable segment to the half-ring cable, the elastic modulus and strength of the SMA are proportionally reduced to ensure that the SMA system is in the transverse direction and to ensure that the SMA body is consistent in the transverse recovery force shift system.

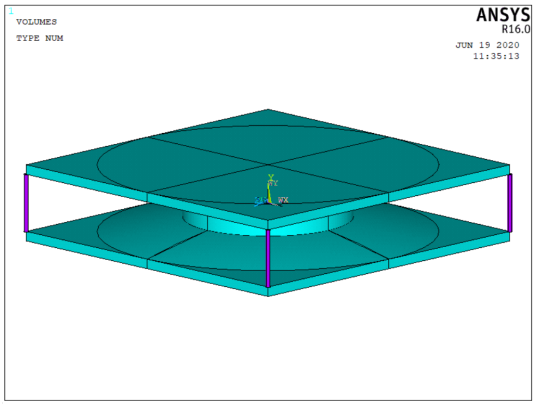

Figure 9. Finite element model of SMA-negative stiffness hyperboloid shock absorber.

The bottom surface of the lower plate adopts fixed constraints. Before horizontal displacement loading, apply vertical pressure on the top surface of the upper plate. To keep the top plate of the device in a horizontal relationship with the bottom plate during the movement process, the Y-direction freedom of the nodes on the top surface of the upper plate is set up with centralized coupling, the Z-direction displacement is fixed, and the X-direction is applied with a reciprocating horizontal displacement load. The friction factor between the slider and the surface is taken as 0.02. To check the effect of the negative stiffness device, an SMA-negative stiffness hyperboloid shock absorber with a curved surface radius of 3 m was selected. A vertical load of 3000 kN is applied, and the loading curve is shown in Figure 10. The comparison of the restoring force-displacement hysteresis curves of the negative stiffness hyperboloid shock absorber and the SMA-negative stiffness hyperboloid shock absorber in the horizontal direction is shown in Figure 11. The hysteresis curve of the SMA negative stiffness hyperboloid shock absorber is very different from that of negative stiffness. First of all, the slope direction of the restoring force of the negative stiffness hyperboloid shock absorber is negative, and the slope direction of the restoring force of the SMA negative stiffness hyperboloid shock absorber is positive, which corresponds to the previous principle of the SMA negative stiffness hyperboloid shock absorber. The slope of the hysteresis curve of the negative stiffness hyperboloid shock absorber is negative, the slope of the SMA hysteresis curve is positive, and the slope of the hysteresis curve of the SMA negative stiffness hyperboloid shock absorber is the superposition of the two. It can also be seen from the figure that the maximum restoring force of the SMA negative stiffness hyperboloid shock absorber is greater than the maximum restoring force of the negative stiffness hyperboloid shock absorber. This is because SMA provides nonlinear restoring force, and SMA acts as a limiter effect.

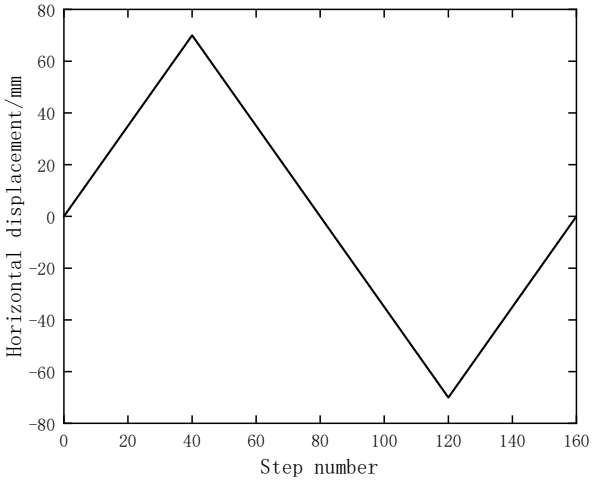

Figure 10. Loading curve.

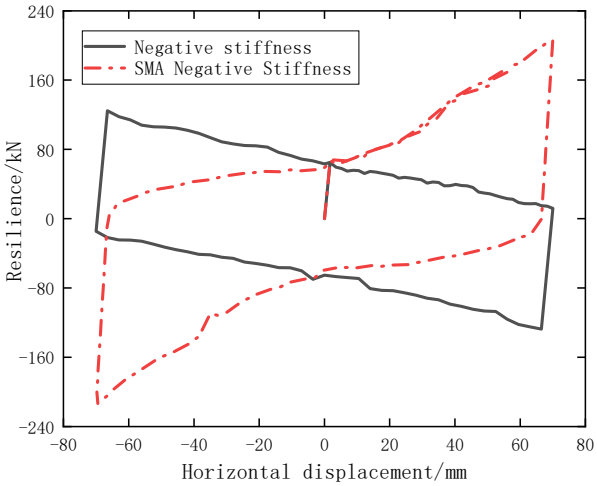

Figure 11. Hysteresis curves of negative stiffness hyperboloid isolator and SMA-negative stiffness hyperboloid isolator.

3.3. Parametric Analysis

3.3.1. Variation of Mechanical Properties with Radius R

To discover the influence law of each key design parameter on the SMA-negative stiffness hyperboloid shock absorber, different key design parameters were selected and their mechanical behaviors were compared and studied. The selected key design parameters are surface radius *R*, horizontal displacement amplitude, SMA cable cross-sectional area, vertical load, and hyperboloid shape.

Select the vertical load as 3000 kN. When the horizontal displacement amplitude is 70 mm, the mechanical properties of the SMA-negative stiffness hyperboloid shock absorber under different surface radii *R* are shown in Figure 12. It can be seen from Figure 12 that the smaller the negative stiffness surface radius *R*, the greater the negative stiffness generated by the negative stiffness device, and the smaller the restoring force, which indicates that the internal force response of the structure decreases with the decrease in the surface radius. When designing the bearing, if conditions permit, the stiffness of the shock absorber can be optimized by adjusting the radius of the curved surface. In terms of energy dissipation capacity and damping ratio, the effect of the surface radius is small.

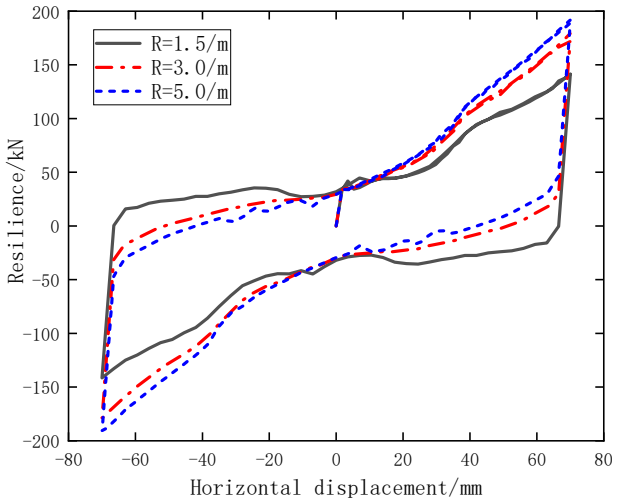

Figure 12. Hysteresis curves of SMA-negative stiffness hyperboloid shock absorber with different surface radii.

3.3.2. Variation of Mechanical Properties with Horizontal Displacement

Select the vertical load as 3000 kN. The mechanical properties of the SMA-negative stiffness hyperboloid shock absorber at different horizontal displacements are shown in Figure 13. It can be seen from Figure 13 that the stiffness of the SMA-negative stiffness hyperboloid shock absorber gradually increases, which can meet the seismic performance requirements under different earthquakes: high shock absorption efficiency during small and medium earthquakes and good limiting effect during strong earthquakes.

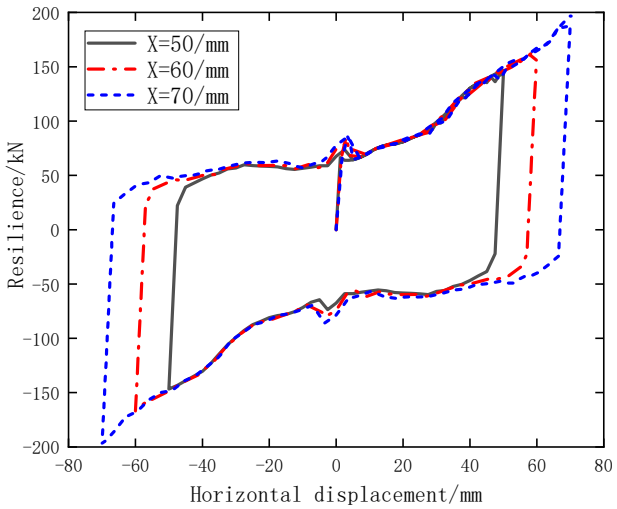

Figure 13. Hysteresis curves of SMA-negative stiffness hyperboloid shock absorber at different horizontal displacements.

3.3.3. Variation of Mechanical Properties with Cross-Sectional Area of SMA Cable

Select the vertical load as 3000 kN. The mechanical properties of the SMA-negative stiffness hyperboloid shock absorber with different SMA cable cross-sectional areas are shown in Figure 14. With the increase of the cross-sectional area of the SMA cable, on the one hand, the shear stiffness of the device increases, and the limit capacity increases; on the other hand, the internal force response of the structure increases. With the increase in the amount of SMA cable, the energy consumption capacity of the shock absorber per cycle increases. On the one hand, this is due to the additional damping of the flag-shaped constitutive structure of the SMA material; on the other hand, the energy dissipation

capacity of the friction surface of the bearing increases because of the increase in the vertical component force of the cable.

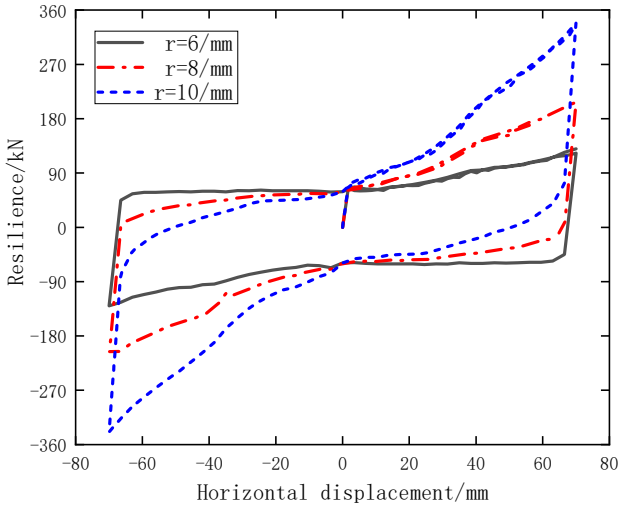

Figure 14. Hysteresis curves of SMA-negative stiffness hyperboloid shock absorber with different SMA numbers.

3.3.4. Variation of Mechanical Properties with Vertical Pressure

To study the mechanical properties of the SMA-negative stiffness hyperboloid shock absorber under different vertical pressures W, vertical loads of 1500 kN, 2500 kN, and 3500 kN were selected for analysis. When the horizontal displacement amplitude is 70 mm, the mechanical behavior of the device is shown in Figure 15. When the vertical loads are 1500 kN, 2500 kN, and 3500 kN, the energy consumption per unit cycle is 22,016 J, 28,368 J, and 34,540 J, respectively, and the damping ratios are 26.2%, 37.0%, and 47.4%, respectively. It can be seen that the larger the vertical pressure W, the larger the area of the hysteresis curve, and the stronger the energy dissipation capacity of the SMA-negative stiffness hyperboloid shock absorber.

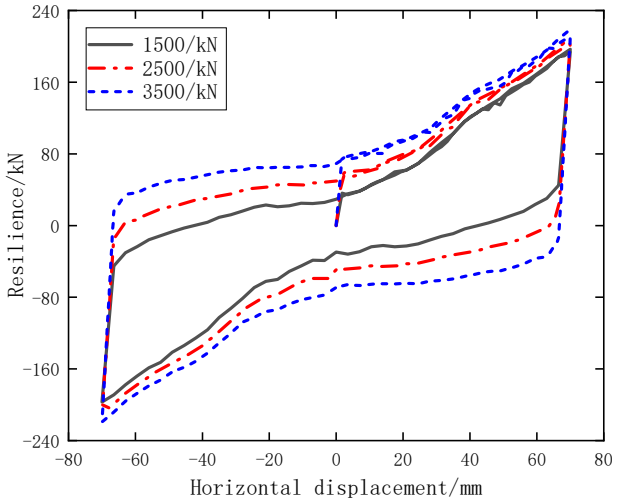

Figure 15. Hysteresis curves of SMA-negative stiffness hyperboloid shock absorber at different vertical pressures.

3.3.5. Effect of Hyperboloid Shape on Mechanical Properties

To further study the influence of different curved surface shapes on the stiffness of the shock absorber, the positive and negative stiffness of curved surfaces and flat planes with a radius of 2 m were selected for research. Select the vertical load as 3000 kN. When

the horizontal displacement amplitude is 70 mm, the restoring force and displacement curves of the three shock absorbers are shown in Figure 16; it can be seen that the three curved surfaces affect the stiffness of the device. The stiffness of the supports generated by the three surfaces is negative stiffness surface, plane, and positive stiffness surface in order from small to large. Compared with the SMA positive stiffness hyperboloid shock absorber, the SMA negative stiffness hyperboloid shock absorber reduces the restoring force by 42.6%, which can effectively reduce the internal force response of the structure.

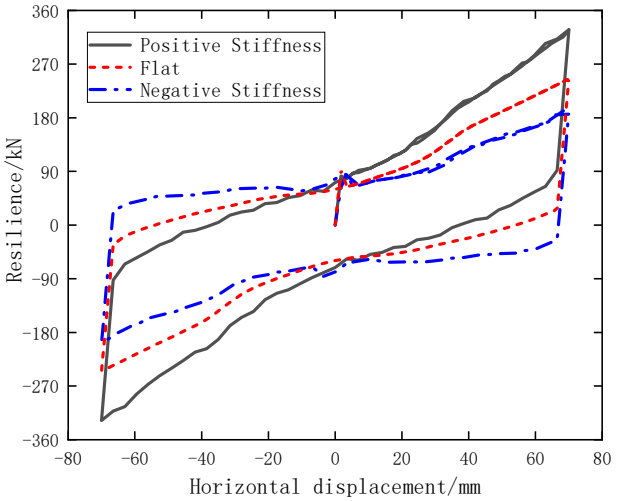

Figure 16. Hysteresis curve of SMA positive stiffness, flat, negative stiffness shock absorber.

4. Shock Absorption Performance Analysis

The SAP2000 finite element model of a 4 × 30 m prestressed concrete continuous girder bridge is shown in Figure 17. The main beam section is a single box with multiple chambers (see Figure 18). Double-column pier, with a tie beam in the middle of the pier. The height of the abutments is 2.5 m, and there are four cast-in-place piles under each abutment. The main girder adopts C50 concrete, and the pile foundation, abutment, and tie beam adopt C30 concrete. To compare and analyze the influence of different supports, the seismic analysis of the positive stiffness, plane, and negative stiffness damping devices of the SMA cable was carried out, respectively. The radius of the curved surface of the positive and negative stiffness SMA shock mounts is 3 m.

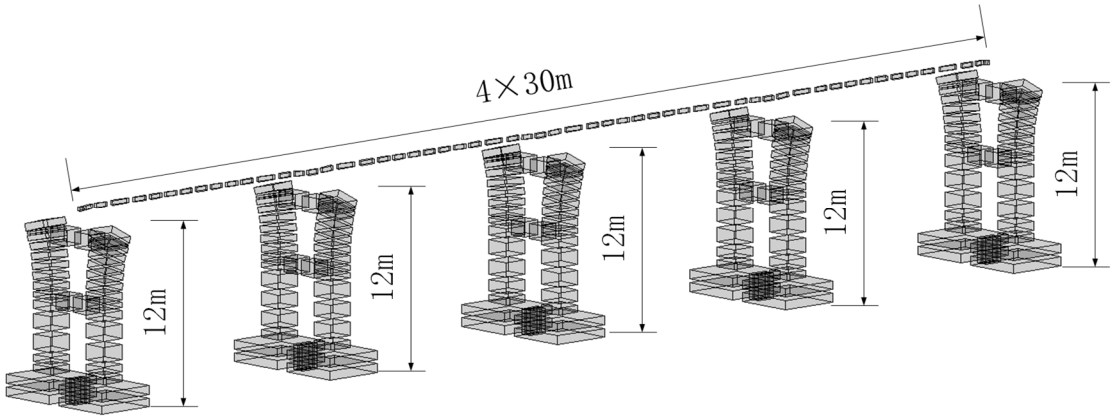

Figure 17. Finite element model.

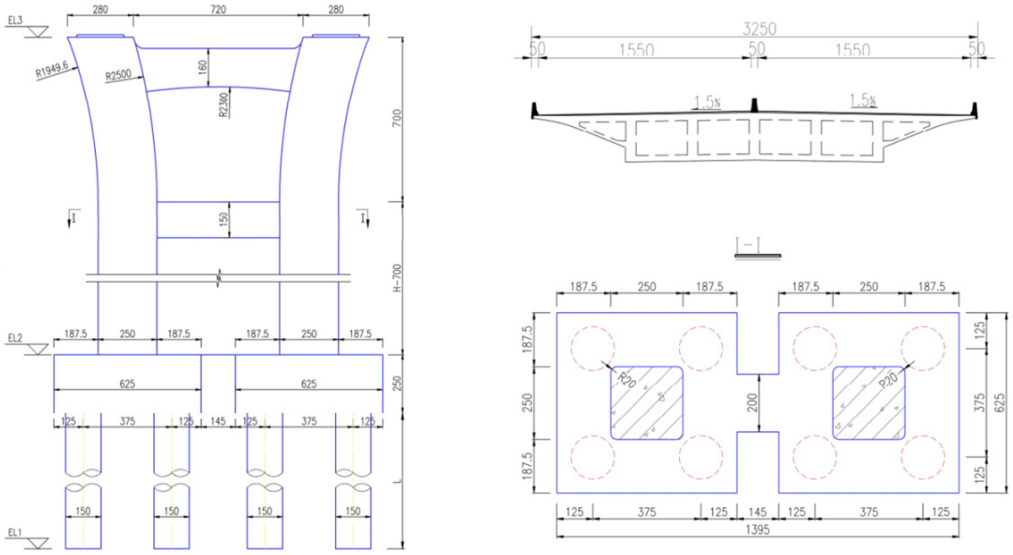

Figure 18. Dimensions of bridge piers, caps and main beams (unit: mm).

4.1. Finite Element Simulation

The finite element model of the full bridge is established based on SAP2000 software. The main beams and bridge piers are simulated by elastic frame elements. The pile-soil interaction is simulated with three rotational and three translational six-spring elements. Since the bridge is a concrete structure, the damping ratio is taken as 0.05. Figure 19, (a) shows the elastic element, (b) shows the plastic element, and (c) shows the constitutive relationship of SMA cable formed by the superposition of elastic element and plastic element. The combination method of the two connection elements is the superposition of the restoring force at the same displacement. The part of the negative stiffness hyperboloid shock absorber is simulated by Plastic (Wen) unit and a linear connection unit with a negative slope; the plane shock absorber is simulated by Plastic (Wen); the positive stiffness hyperboloid shock absorber is simulated by Plastic (Wen) and a slope of positive line element simulation.

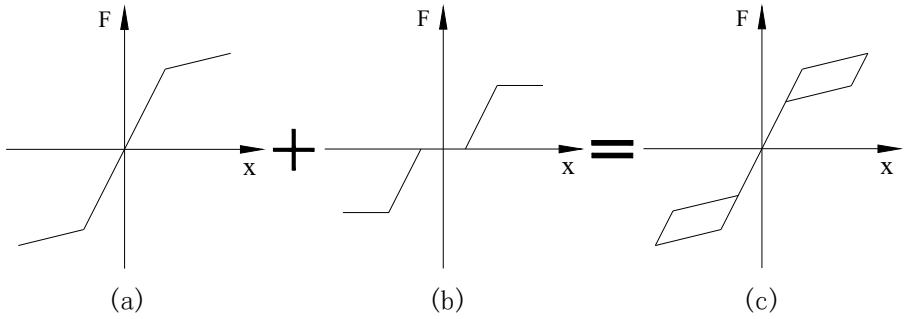

Figure 19. SMA cable overlay.

To verify the correctness of the shock absorber simulation in SAP2000 software, Figure 20 compares the hysteresis curves obtained by SAP2000 and ANSYS software to simulate the shock absorber. Overall, the restoring force models calculated by the two software for the shock absorber are the same, which shows that SAP2000 can well-simulate the constitutive relationship of the shock absorber.

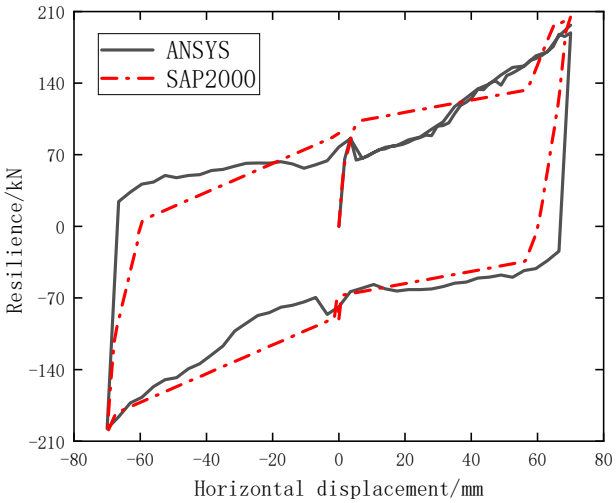

Figure 20. Restoring force-displacement relationship of SMA-negative stiffness isolator.

4.2. Selection of Seismic Waves

According to the earthquake safety evaluation report, the basic fortification intensity of the bridge is 7 degrees, and it is a Class II site. Three near-field seismic waves with a single directional component were selected from the PEER seismic database. According to the design response spectrum of the site where the bridge is located, based on the SeismoMatch software, the selected three seismic waves are scaled. The response spectrum of the three scaled seismic waves is compared with the design response spectrum, as shown in Figure 21. The scaled seismic waves are used as seismic waves for time history analysis and are input along the longitudinal bridge direction. The time history analysis results in this paper are all longitudinal bridge responses.

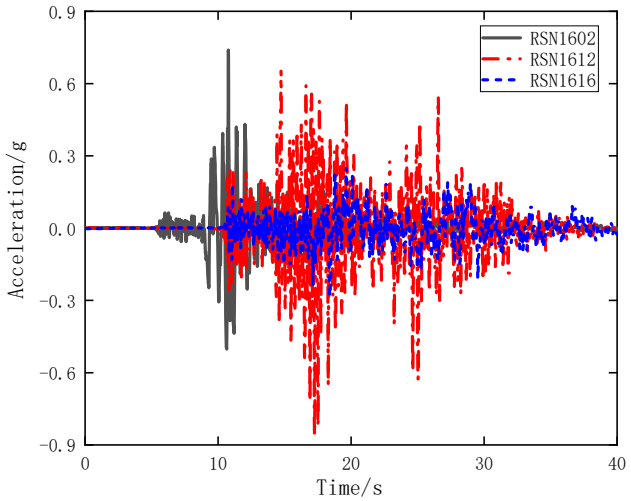

Figure 21. Time-history curve of near-field vibration acceleration.

4.3. Earthquake Response Comparative Analysis

4.3.1. Bearing Displacement Response

Under three kinds of near-field vibrations, for the bridge structure system with positive stiffness, plane, and negative stiffness SMA damping device respectively, the displacement history curve of the right bearing of the middle pier is shown in Figure 22, and the maximum displacement of the bearing is shown in Table 1. It can be seen from Figure 22 that under the action of near-field vibration, the positive stiffness, plane, and negative stiffness of SMA shock absorbers can better control the displacement of the bearing. It can be seen from Table 1 that the bearing displacement of the SMA-negative stiffness hyperboloid damping

bridge is slightly larger than that of the SMA plane damping bridge and the SMA positive stiffness hyperboloid damping bridge. This shows that compared with the commonly used SMA shock absorber with positive stiffness, the SMA shock absorber designed with the concept of negative stiffness will not cause excessive displacement growth better.

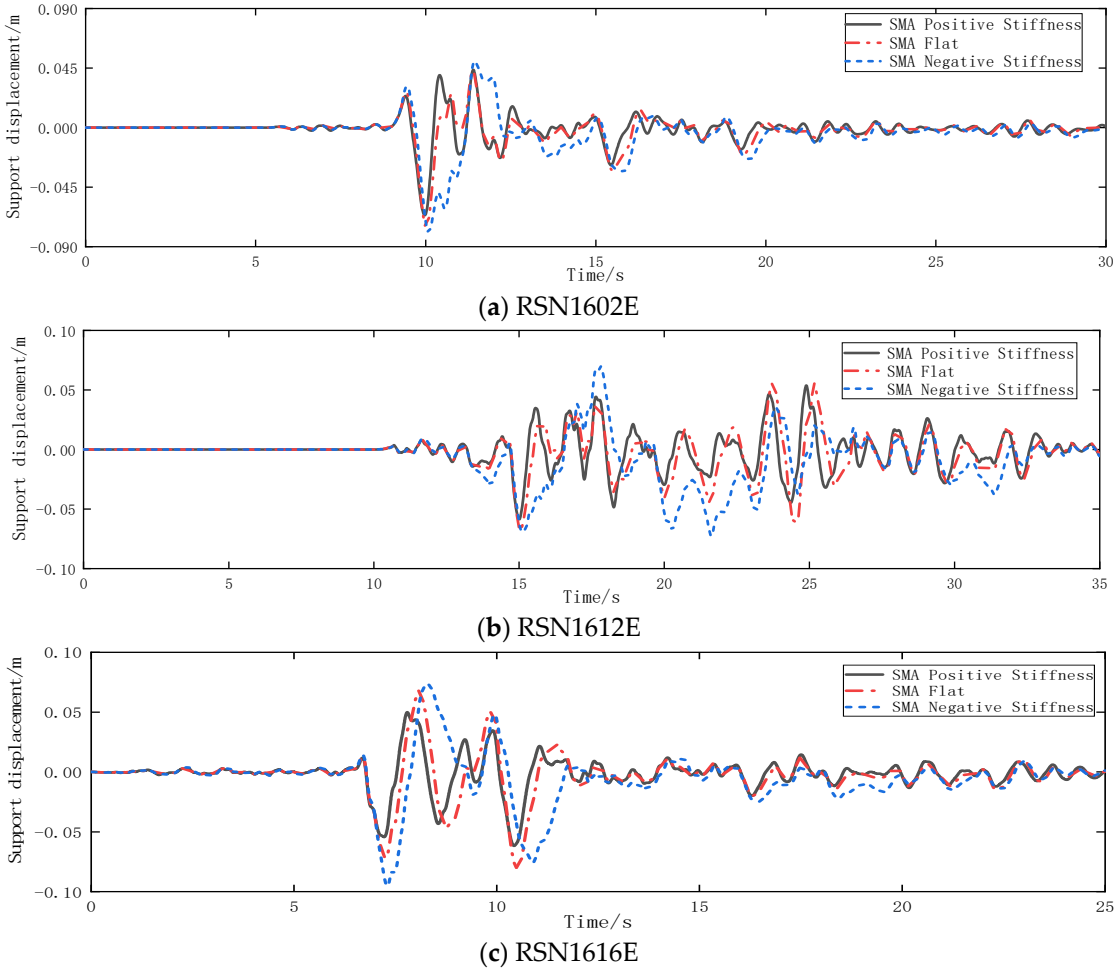

Figure 22. Time-history curve of bearing displacement under the action of near-field vibration.

Table 1. The displacement amplitude and damping rate of the bearing under the action of near-field vibration.

Seismic Wave		Positive Stiffness	Flat	Negative Stiffness
RSN1602E	Amplitude/mm	66.35	75.80	78.78
RSN1612E	Amplitude/mm	58.64	68.25	72.78
RSN1616E	Amplitude/mm	61.75	81.30	95.58

4.3.2. Support Hysteresis Curve

Under three kinds of near-field vibrations, the hysteresis curves of the bearings on the right side of the middle pier are shown in Figure. It can be seen from Figure 23 that the positive stiffness, plane and negative stiffness of SMA hyperboloid shock absorbers can effectively limit the displacement of the bearing under the action of near-field vibration. Among them, the SMA-negative stiffness hyperboloid shock absorber bearing has the smallest shear force, the SMA plane shock absorber bearing has a slightly larger shear force, and the SMA positive stiffness hyperboloid shock absorber bearing has the largest shear force. Compared with the SMA positive stiffness, the sheer force of the SMA negative stiffness bearing is generally reduced, which fully reflects the superiority of the negative

stiffness design concept. It can be seen from Table 2 that the SMA negative rigidity dual -surface shock absorption device has the smallest shear support, followed by SMA plane shock absorption device support, SMA positive rigid dual -curved shock absorption device has the largest shear, three near the field near the field The reduction of the shear power of the mid -seismic wave was 789 kN, 836 kN, and 364 kN, respectively.

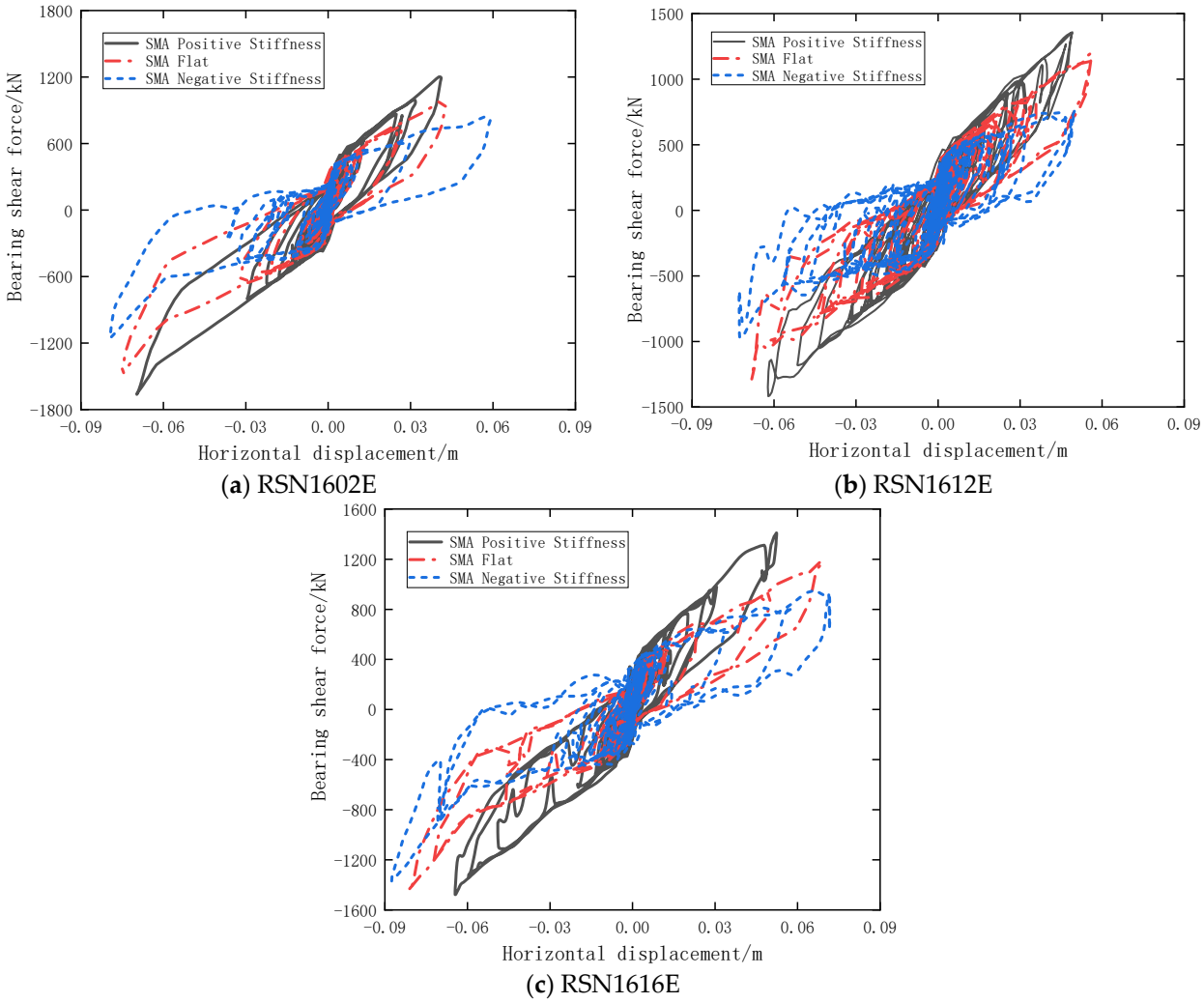

(**a**) RSN1602E (**b**) RSN1612E

(**c**) RSN1616E

Figure 23. Time-history curve of bearing shear force under the action of near-field vibration.

Table 2. Shear force amplitude and damping rate of bearing under the action of near-field vibration.

Seismic Wave		Positive Stiffness	Flat	Negative Stiffness
RSN1602E	Amplitude/kN	1695	1512	906
RSN1612E	Amplitude/kN	1599	1298	763
RSN1616E	Amplitude/kN	1689	1535	1325

4.3.3. Pier Bottom Bending Moment Response

Under the action of three kinds of near-field vibrations, the bending moment his-tory curves of the bottom of the middle pier right cap of the three kinds of shock-absorbing bridge structural systems are shown in Figure 24. It can be seen from Figure 24 that under the action of near-field vibration, the bending moment of the platform bottom of the positive stiffness and plane SMA shock-absorbing bridge structural system is larger than that of the negative stiffness bearing. The SMA positive stiffness hyperboloid shock absorbing bridge system produces the largest bearing plat-form bottom bending moment, followed by the

SMA plane shock absorbing bridge sys-tem, while the SMA-negative stiffness hyperboloid shock absorbing bridge system has the smallest bearing platform bottom bending moment. It can be seen from Table 3 that the bending moment at the bottom of the SMA negative stiffness hyperboloid damping pier is the smallest, followed by the bending moment at the bottom of the SMA plane damping pier, and the bending moment at the bottom of the SMA positive stiffness hyperboloid damping pier is the largest. The reduction of the bending moment at the bottom of the pier in the three near-field seismic waves is 6744 kN·m, 5471 kN·m and 5947 kN·m.

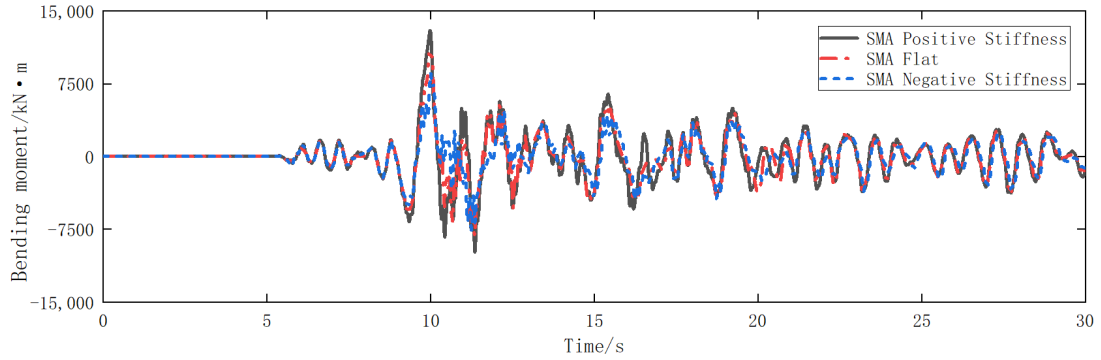

(**a**) RSN1602E

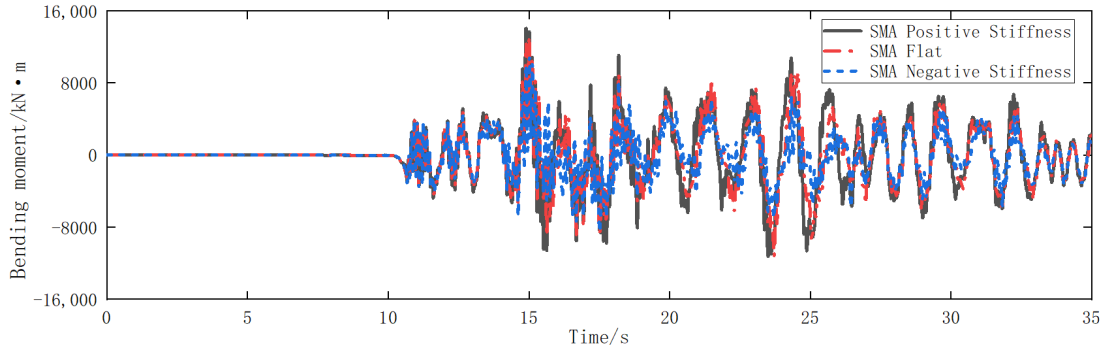

(**b**) RSN1612E

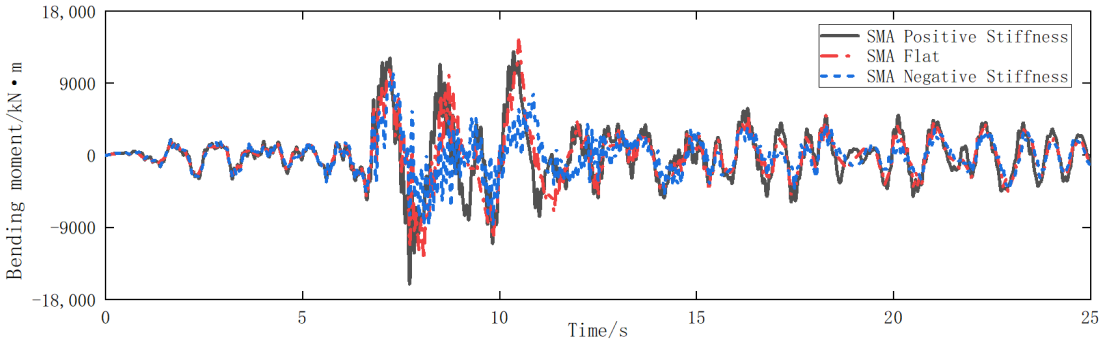

(**c**) RSN1616E

Figure 24. Time-history curve of pier bottom bending moment under the action of near-site vibration.

Table 3. Bending moment amplitude and damping rate of pier bottom under near-site vibration.

Seismic Wave		Positive Stiffness	Flat	Negative Stiffness
RSN1602E	Amplitude/kN·m	13,340	11,224	6596
RSN1612E	Amplitude/kN·m	14,866	13,166	9395
RSN1616E	Amplitude/kN·m	16,084	14,628	10,137

5. Conclusions

1. SMA negative stiffness hyperboloid isolation device can provide self resetting ability for bridges. Compared with SMA positive stiffness hyperboloid isolation device, SMA negative stiffness hyperboloid isolation device can reduce the bearing displacement, increase the damping ratio and energy dissipation capacity, and partially reduce the internal force response of the substructure.
2. SMA negative stiffness hyperboloid damping device reduces the bending moment at the bottom of the pier when it vibrates near the site. Compared with the three damping devices, the negative stiffness hyperboloid damping reduces the stiffness of the bridge, resulting in the reduction of the bending moment at the bottom of the pier and the amplitude of the bearing shear force.
3. The magnitude of the negative stiffness of the SMA-negative stiffness hyperboloid shock absorber depends on the radius of the curved surface. The smaller the surface radius, the greater the negative stiffness effect. The stiffness optimization of the shock absorber can be achieved by adjusting the radius of the curved surface.
4. With the increase of the cross-sectional area of the SMA cable, although the equivalent secant stiffness of the SMA-negative stiffness hyperboloid shock absorber increases, the energy dissipation capacity and the limit capacity increase. This will also increase the internal force response of the structure. With the increase of vertical load, the energy dissipation capacity of the SMA-negative stiffness hyperboloid shock absorber increases.

Author Contributions: Conceptualization, H.C. and S.C.; methodology, H.C. and S.C.; validation, H.C.; formal analysis, L.L.; investigation, H.C.; resources, L.J. and J.L.; data curation, L.L.; writing—original draft preparation, H.C. and S.C.; writing—review and editing, H.C. and L.J.; visualization, J.L.; supervision, L.L. and J.L.; project administration, H.C. and S.C. All authors have read and agreed to the published version of the manuscript.

Funding: The project was financially supported by the National Natural Science Foundation of China (Grants 52178124, 51608136, 51278134); Natural Science Foundation of Guangdong Province (Grant 2020A1515010231, 2022A1515011250), Science and Technology Planning Project of Guangdong Province (Grant 2020A1414010271).

Institutional Review Board Statement: Not applicable.

Informed Consent Statement: Not applicable.

Data Availability Statement: The data that support the findings of this study are available from the corresponding authors upon reasonable request.

Conflicts of Interest: The authors declare no conflict of interest.

References

1. Housner, G.W.; Thiel, C.C., Jr. The continuing challenge: Report on the performance of state bridges in the northridge earthquake. *Earthq. Spectra* **1995**, *11*, 607–636. [CrossRef]
2. Bruneau, M.; Wilson, J.C.; Tremblay, R. Performance of steel bridges during the 1995 Hyogo-ken Nanbu (Kobe, Ja). *Can. J. Civ. Eng.* **1996**, *23*, 678–713. [CrossRef]
3. Sun, X.D.; Tao, X.X.; Duan, S.S.; Liu, C.Q. Kappa (k) derived from accelerograms recorded in the 2008 Wenchuan mainshock, Sichuan, China. *J. Asian Earth Sci.* **2013**, *73*, 306–316. [CrossRef]
4. Liu, C.Q.; Fang, D.J.; Zhao, L.J. Reflection on earthquake damage of buildings in 2015 Nepal earthquake and seismic measures for post-earthquake reconstruction. *Structures* **2021**, *30*, 647–658. [CrossRef]
5. Li, J.Z.; Peng, T.; Yan, X. Damage investigation of girder bridges under the Wenchuan earthquake and corresponding seismic design recommendations. *Earthq. Eng. Eng. Vib.* **2008**, *7*, 337–344. [CrossRef]
6. Raheem, S.E.A. Pounding mitigation and unseating prevention at expansion joints of isolated multi-span bridges. *Eng. Struct.* **2009**, *31*, 2345–2356. [CrossRef]
7. Karalar, M.; Padgett, J.E.; Dicleli, M. Parametric analysis of optimum isolator properties for bridges susceptible to near-fault ground motions. *Eng. Struct.* **2012**, *40*, 276–287. [CrossRef]
8. Huang, Z.; Li, H.N.; Fu, X. Optimum design of a re-centering deformation-amplified SMA damper. *Eng. Mech.* **2019**, *36*, 202–210.

9. Hu, S.J.; Gu, Q.; Jiang, G.Q.; Xiong, J.G. Experimental study on seismic performance for an innovative self-centering SMA brace. *Eng. Mech.* **2021**, *38*, 109–118.
10. Andrawes, B.; DesRoches, R. Comparison between shape memory alloy seismicre strainers and other bridge retrofit devices. *J. Bridge Eng.* **2007**, *12*, 700–709. [CrossRef]
11. DesRoches, R.; Pfeifer, T.; Leon, R.T.; Lam, T. Full-scale tests of seismic cable restrainer retrofits for simply supported bridges. *J. Bridge Eng.* **2003**, *8*, 191–198. [CrossRef]
12. Choi, E.; Nam, T.H.; Oh, J.T.; Cho, B.S. An Isolation Bearing for Highway Bridges Using Shape Memory Alloys. In Proceedings of the International Conference on Martensitic Transformations (ICOMAT05), Shanghai, China, 13–17 January 2005.
13. Shinozuka, M.; Chaudhuri, S.R.; Mishra, S.K. Shape memory-alloy supplemented lead rubber bearing (SMA-LRB) for seismic isolation. *Probabilist. Eng. Mech.* **2015**, *41*, 34–45. [CrossRef]
14. Wang, J.Q.; Li, S.; Dezfuli, F.H.; Alam, M.S. Sensitivity analysis and multi-criteria optimization of SMA cable restrainers for longitudinal seismic protection of isolated simply supported highway bridges. *Eng. Struct.* **2019**, *189*, 509–522. [CrossRef]
15. Liang, D.; Zheng, Y.; Fang, C.; Yam, M.C.H.; Zhang, C.T. Shape memory alloy (SMA)-cable-controlled sliding bearings: Development, testing, and system behavior. *Smart Mater. Struct.* **2020**, *29*, 085006. [CrossRef]
16. Wang, B.; Zhu, S.Y.; Casciati, F. Experimental study of novel self-centering seismic base isolators incorporating superelastic shape memory alloys. *J. Struct. Eng.* **2020**, *146*, 1–16. [CrossRef]
17. Cao, S.S.; Ozbulut, O.E.; Shi, F.; Deng, J.D. Experimental and numerical investigations on hysteretic response of a multi-level SMA/lead rubber bearing seismic isolation system. *Smart Mater. Struct.* **2022**, *31*, 035024. [CrossRef]
18. Cao, S.S.; Ozbulut, O.E.; Shi, F.; Deng, J.D. An SMA cable-based negative stiffness seismic isolator: Development, experimental characterization, and numerical modeling. *J. Intel. Mat. Syst. Str.* **2022**, *33*, 1819–1833. [CrossRef]
19. Cao, S.S.; Yi, J. Shape memory alloy-spring damper for seismic control and its application to bridge with laminated rubber bearings. *Adv. Struct. Eng.* **2021**, *24*, 3550–3563. [CrossRef]
20. Cao, S.S.; Ozbulut, O.E.; Wei, S.W.; Sun, Z.; Deng, J.D. Multi-level SMA/lead rubber bearing isolation system for seismic protection of bridges. *Smart Mater. Struct.* **2020**, *29*, 055045. [CrossRef]
21. Wang, H.; Cao, S.S. Multi-Level Performance Shape Memory Alloy-Based Lead Rubber Bearing. In Proceedings of the 3rd International Conference on Smart City and Systems Engineering (ICSCSE), Xiamen, China, 29–30 December 2018.
22. Han, Q.; Liang, X.; Wen, J.N.; Zhang, J.; Du, X.L.; Wang, Z.Q. Multiple-variable frequency pendulum isolator with high-performance materials. *Smart Mater. Struct.* **2020**, *29*, 075002. [CrossRef]
23. Hiramoto, K.; Matsuoka, T.; Sunakoda, K. Simultaneous optimal design of the structural model for the semi-active control design and the model-based semi-active control. *Struct. Control Health* **2014**, *21*, 522–541. [CrossRef]
24. Liu, C.Q.; Fang, D.J.; Zhao, L.J.; Zhou, J.H. Seismic fragility estimates of steel diagrid structure with performance-based tests for high-rise buildings. *J. Build. Eng.* **2022**, *52*, 104459. [CrossRef]
25. Zhao, J.; Zhao, Y.; Ruan, X.H.; Gong, X.L.; Zhang, X.C. Experimental research on the seismic properties of shear wall reinforced with high-strength bars and magnetorheological dampers. *Struct. Control. Health* **2021**, *28*, e2779. [CrossRef]
26. Bani-Hani, K.A.; Sheban, M.A. Semi-active neuro-control for base-isolation system using magnetor heological (MR) dampers. *Earthq. Eng. Struct. Dyn.* **2006**, *35*, 1119–1144. [CrossRef]
27. Li, H.; Liu, M.; Ou, J.P. Negative stiffness characteristics of active and semi-active control systems for stay cables. *Struct. Control Health* **2008**, *15*, 120–142. [CrossRef]
28. Iemura, H.; Igarashi, A.; Pradono, M.H.; Kalantari, A. Negative stiffness friction damping for seismically isolated structures. *Struct Control Health* **2006**, *13*, 775–791. [CrossRef]
29. Attary, N.; Symans, M.; Nagarajaiah, S.; Reinhorn, A.M.; Constantinou, M.C.; Sarlis, A.A.; Pasala, D.T.R.; Taylor, D. Numerical simulations of a highway bridge structure employing passive negative stiffness device for seismic protection. *Earthq. Eng. Struct. Dyn.* **2015**, *44*, 973–995. [CrossRef]
30. Attary, N.; Symans, M.; Nagarajaiah, S.; Reinhorn, A.M.; Constantinou, M.C.; Sarlis, A.A.; Pasala, D.T.R.; Taylor, D. Performance evaluation of negative stiffness devices for seismic response control of bridge structures via experimental shake table tests. *J. Earthq. Eng.* **2015**, *19*, 249–276. [CrossRef]
31. Deng, J.D.; Hu, F.L.; Ozbulut, O.E.; Cao, S.S. Verification of Multi-level SMA/lead rubber bearing isolation system for seismic protection of bridges. *Soil. Dyn. Earthq. Eng.* **2020**, *161*, 107380. [CrossRef]
32. Shao, C.X.; Cao, S.S. Test and development of SMA-based negative stiffness isolation device. *Adv. Struct. Eng.* **2022**. [CrossRef]
33. Chang, H.H.; Cao, S.S.; Ji, H.Y. SMA Negative Stiffness Damper. In Proceedings of the 2020 International Conference on Intelligent Transportation, Big Data & Smart City (ICITBS), Vientiane, Laos, 11–12 January 2020.
34. Sun, T.; Lai, Z.L.; Nagarajaiah, S.; Li, H.N. Negative stiffness device for seismic protection of smart base isolated benchmark building. *Struct. Control Health* **2017**, *24*, e1968. [CrossRef]
35. Yang, Q.R.; Ran, M.L.; He, W.F.; Yu, W.X.; Liu, W.G. Study on seismic response of isolated structure based on damping negative stiffness device. *J. Vib. Eng.* **2018**, *31*, 920–929.
36. Liu, M.; Zhou, P.; Li, H. Novel self-centering negative stiffness damper based on combination of shape memory alloy and prepressed springs. *J. Aerosp. Eng.* **2018**, *31*, 04018100. [CrossRef]
37. Iemura, H.; Pradono, M.H. Simple algorithm for semi-active seismic response control of cable-stayed bridges. *Earthq. Eng. Struct. Dyn.* **2005**, *34*, 409–423. [CrossRef]

38. Iemura, H.; Pradono, M.H. Advances in the development of pseudo-negative-stiffness dampers for seismicre sponse control. *Struct. Control Health* **2009**, *16*, 784–799.
39. Ozbulut, O.E.; Daghash, S.; Sherif, M.M. Shape memory alloy cables for structural applications. *J. Mater. Civ. Eng.* **2016**, *28*, 04015176. [CrossRef]
40. Auricchio, F.; Taylor, R.L. Shape-memory alloys: Modelling and numerical simulations of the finite-strains uperelastic behavior. *Comput. Methods Appl. Mech. Eng.* **1997**, *143*, 175–194. [CrossRef]